Homotruxene, obtained by trimerization of 1-tetralone, is unique as a hydrocarbon in showing both triplet and singlet afterglow upon irradiation under ambientconditions.

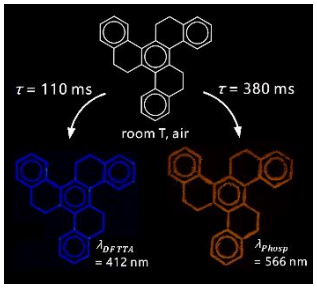

Persistent solid-state phosphorescence and delayed fluorescenceat room temperature from a twisted hydrocarbon

CristianA.M. Salla,[a]Giliandro Farias,[b]Mathieu Rouzières,[c]Pierre Dechambenoit,[c]Fabien Durola,[c]Harald Bock,*[c] Bernardo de Souza,*[b]and Ivan H. Bechtold*[a]
published in*Angew. Chem. Int. Ed.* **2019***, 58,* 6982-6986; DOI: 10.1002/anie.201901672

[a] Departamento de Física, Universidade Federal de Santa Catarina 88040-900 Florianópolis, SC, Brazil; ivan.bechtold@ufsc.br
[b] Departamento de Química, Universidade Federal de Santa Catarina 88040-900 Florianópolis, SC, Brazil; bernardo.souza@ufsc.br
[c] Centre de Recherche Paul Pascal, CNRS & Université de Bordeaux, 115, av. Schweitzer, 33600 Pessac, France; bock@crpp-bordeaux.cnrs.fr

Abstract: The dehydrating cyclotrimerization of 1-tetralone in the presence of titanium tetrachloride at high temperature leads to homotruxene, a nonplanararene in which the twist angles between its three outer benzene rings and the central benzene are stabilized by ethylene bridges. This non-planar configuration allows for pronounced spin-orbit coupling and a high triplet energy, leading to room temperature phosphorescence in air with a lifetimeof 0.38 s and a quantum yield of 5.6%, cleanly visible to the human eye after switch-off of excitation. Triplet-triplet annihilation is found to simultaneously lead to an intense delayed fluorescence, unprecedented from a pure hydrocarbon at ambient conditions, with a lifetimeof 0.11 s.

Although the phosphorescence and, to a lesser extent, delayed fluorescence(DF) of polycyclic aromatic hydrocarbons in host matrices has been studied in the middle of the last century at low as well as at room temperature,[1-6]this class of materials is notably absent from the recent surge of interest in room-temperature phosphorescence (RTP) and DFfrom single-component crystalline organic materials.[7,8] Recent metal-free RTP and DF materials either contain heavy atoms such as bromine to facilitate singlet-triplet intersystem crossing (ISC), or polarizing heteroatoms such as oxygen or nitrogenthat induce charge-transfer states.[7]Simple prototypical examples are dibromo-biphenyl**1**,[9]benzophenone**2**[9]and carbazolylbenzoate**3**[10]with RTP quantum yieldsΦ in the crystalline state of 14%, 16% and 2.1 %, and RTP lifetimes $\tau$of 0.81ms, 0.31 ms and 0.8 s. These data illustrate the obvious: whilst there is of course no linear correlation between yield and lifetime, a high $\Phi$is much harder to achieve if phosphorescence is persistent (**3**),than if lifetimes arein or below the millisecond range(**1**, **2**) and thus can more easily compete with nonradiative deactivation. Short-lived RTP with Φ near unity has been obtained with Ir and Pt complexes[11] and with a benzene bearing six arylthio substituents.[12]Innovative approaches for the improvement of RTP via intermolecular interactions are crystallization-induced phosphorescence,[13] halogen bonding in co-crystals,[14] aggregation-induced ISC,[15]complexation-induced RTP in solution[16] and emission from H-aggregates.[17]

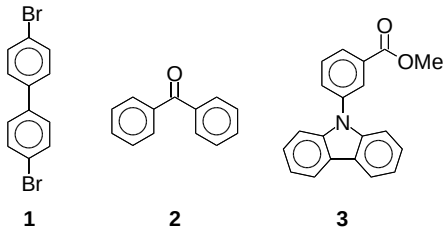

1 **2** **3**

Scheme 1. Exemplary metal-free materials whose crystals show RTP.

In general, electronic transitions between non-coplanar (orthogonal or tilted) orbitals are necessary to allow forspin-orbit coupling(SOC),[18,19]but the vast majority of polycyclic aromatic compounds do not present this kind of geometry.However, a hydrocarbon whose persistent solid-state RTPwas noted early is tetraphenylmethane**4**.[20]Itspeculiar three-dimensional structure of four-fold symmetry[21]distinguishes **4** from most polycyclic arenes, who generally show no persistent RTP in the pure crystalline state. Very weak long-lived RTP in the crystal has also been reported[3]for the two C3-symmetric species triphenylene**5**[22]and sym-triphenylbenzene**6**(which is non-planar). Thisfaint persistent RTP can be linked to SOC induced by the twisting of the outer rings, as crystalline**6**adopts a non-planardissymmetric structure where one phenyl substituent tilts out of the central benzene planeintheopposite sense of the other two phenyls, with dihedralangles of+35.1°, -34.5° and-38.4° at the single bonds.[23]

In contrast to the rare reports of persistent RTP from hydrocarbons in the solid state in ambient atmosphere, DF from pure hydrocarbons at room temperature has only been observed under exclusion of oxygen, originating from surface sites.[24]

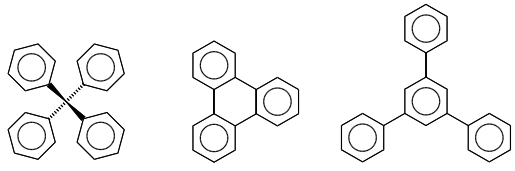

4 **5** **6**

Scheme 2. Hydrocarbons that have been reported to show faint RTP in the crystalline state.

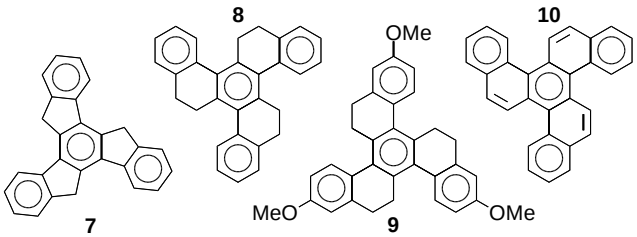

7 **9**

Scheme 3. Planar and twisted rigidified derivatives of triphenylbenzene**6**.

Introducing saturated bridges between the benzene rings of **6** is a means of rigidifying the angle between benzenes at a fixed value, hindering rotational pathways of triplet deactivation without fundamental changes to the chromophore that would result from unsaturated bridges. Truxene**7**, the symmetrically triply methylene-bridged derivative of **6**, is obtained by acid-catalyzed trimerizingcyclodehydration of 1-indanone,[25] similar to the synthesis of **6** from acetophenone.[26] The five-membered rings in **7** force its benzene rings into coplanarity, enhancing conjugation but minimizing the SOC. We could not observe any persistent RTP with a purified commercial sample of **7**.

The six-membered-ring homolog **8** of truxene, for which we propose the short name homotruxene, had not yet been obtained. The ethylene bridges in homotruxene should stabilize the outer benzene rings in an out-of-plane configuration with respect to the central ring, potentially allowing for SOC and phosphorescence. Whilst Pyrko found that its trimethoxy-derivative **9** is formed in 41% yield from 6-methoxy-1-tetralone in the presence of $TiCl_4$ and triethylamine,[27]Hagen and Scott found that unsubstituted 1-tetralone fails to trimerize under similar conditions (giving only a dimer), which led them to design a four- instead of two-step synthesis of the fully aromatized tribenzotriphenylene**10**.[28]

Here we describe a simple path to hydrocarbon**8** and investigate its unprecedented persistent solid-state RTPcombined withDF.

We had to confirm that Pyrko's method fails to give**8**, but trace amounts of **8** could be obtained when using Hünig's base instead of triethylamineand could be isolated due to their ease of crystallization from acetone. This led us to explore harsher reaction conditions to force the trimerization,and we found that **8**could be obtained in an optimized yield of 10% when reacting tetralone with $TiCl_4$ in a molar ratio of 4:1 at 150°C without solvent.Higher temperatures led to purification difficulties without gain in yield, and higher proportions of $TiCl_4$ lowered the yield, presumably due to its diluting effectthat favors dimerization over trimerization. Although the yield of 10% might lookunsatisfactory, it allows the straightforward gram-scale production of easily crystallizing **8** from two extremely cheap reagents. Crystals from acetone proved suitable for structure determination and showed the desired persistent luminescence.

Homotruxene **8** crystallizes in highly symmetrical trigonal crystals, where all dihydronaphthylene units (molecular thirds) are symmetry-related (Figure 1 and ESI). No intermolecular van-der-Waals-contacts are present, i.e. the individualπ-electron systems are insulated from their environment. The torsion angle between the central and any peripheral benzene ring measured over the connecting bond is 32.6° when including the bridge-bearing ortho carbon atoms, and 36.1° when including instead the hydrogen-bearing carbon atoms, giving a mean of 34.3°, close to the average of 36.0° in triphenylbenzene**6**.[23]

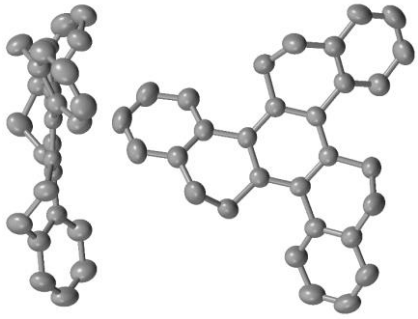

Figure 1. Views of one of two symmetry-related molecules of **8.** Ellipsoids at 90% probability level; hydrogen atoms omitted.

In solution at room temperature, **8** gives an unusual proton NMR spectrum with four strongly broadened aliphatic signals that testify that the four aliphatic protons per bridge are stabilized in distinct environments within a dissymmetric conformation, confirming the partial lock-in of tilt between benzene planes even in solution (Figure S3 in ESI).

In chloroform (Figure 2), **8** shows a main absorption band at 275 nm witha shoulder at 290 nm, and a weaker band at 330 nm with an absorption edge atabout350 nm. In spin-coated film, due to small geometry changes and possibly aggregation effects, the absorption maximum is only slightly shifted to 278 nm, whereas the tail of the absorption spectrum extends to markedly longer wavelengths, with an absorption edge at about400 nm.

When excited in the lower energy absorption band at 340 nm, the prompt emission spectrum in solution consists of only one peak at 412 nm. This emission was found to be 1.6 times more intense in degassed solution under argon (Φ= 8.6%, versusanthracene standard) than under air (5.5%), indicating that part of the emission was quenched by oxygen. This short-wavelength emission could still be observed several ms after the switch-off of excitation, which hinted to a DF related to a triplet excited state.

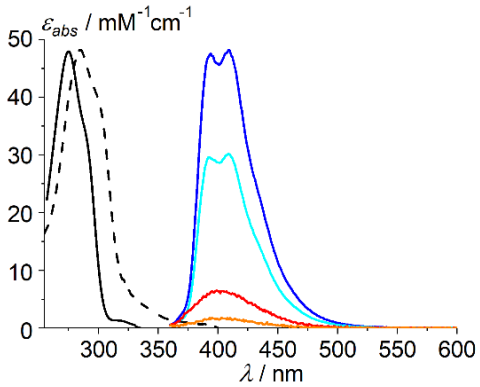

Figure 2. Absorption (black) and emissionspectra (normalized; light blue: under air; dark blue: under argon;red: under argon 0.1 ms after excitation switch-off; orange: same after 1.0 ms) of **8** in 20μM chloroform solution. The dashed line is the normalized solid-stateabsorption.

In contrast to the solution, a longer-wavelength emission is present under continuous excitation in powder or spin coated-film, with a maximum at 566nm and a shoulder at 600 nm.Both the short and long wavelength parts of the emission persist over many ms after excitation switch-off (Figure 3).$\Phi$for the fluorescence in the crystalline powder(at room temperature under air) is, unsurprisingly, much higher than in solution, of35.4%, and Φ of the lower energy peak, subsequently shown to be due to phosphorescence,is 5.6%.Although that is lower than the yields obtained with fast organic RTP materials presenting heteroatoms such as **1** or **2**,[9]$\Phi$of crystalline**8** is excellent for a persistent (τ> 0.1 s) RTP material.The spin-coated film, which may be considered amorphous as it has a smooth surface (RMS roughness of 0.35 nm by AFM)that yields sleek grooves when scratched with a needleand shows no birefringence atpolarizing optical microscopy (Figure S4 in ESI), gives lower yet comparablequantum yieldsΦ, of 26.6% and 2.9%.

Weprobedthe effect of temperature on this dual delayed emission. On cooling from 300 K to 75 K, the intensity of the emission peak at 566 nm increases, which usually occurs in phosphorescence due to the suppression of nonradiative triplet decay,[29]whilst the intensity of the peak at 412 nm decreases. This temperature dependence is usually assigned to as thermally activated DF (TADF), but the gap between the lowest triplet and the lowest excited singlet is 1.02 eV, too high for thermal up-conversion.

In the solid state at room temperature, the emission at 412 nm has a lifetime of 0.11 s, whilst the emission at 566 nm is more persistent, with a lifetime of 0.38 s (Figure S1 in ESI). On cooling, the lifetime of the peak at 566 nm increases, as usually seen for phosphorescence, whereas the lifetime of the peak at 412 nm does not change significantly (Inset of Figure S1 in ESI). This contrasts with what is typically seen in TADF, where at very low temperatures there would be no DF at all. The DF must thus be due to a triplet-triplet annihilation (TTA) process.

To probe further whether the DF is due to a monomolecular (TADF) or a bimolecular (TTA) process, we measured the emission of **8** in a PMMA matrix at different concentrations. The relative emission intensity at 412 nm with respect to the phosphorescence at 566 nm decreases consistently with dilution (Figure S2 in ESI). As the TTA emission depends on the encounter of two triplets, its relative intensity should decrease when varying the concentration from 50% to 1%, whereas no decrease would be expected for TADF. In a consistent mechanism that accounts for prompt fluorescence, delayed fluorescence and phosphorescence, TTA leads to a singlet ground state S_0 and to an excited singlet state that subsequently decays to the ground state by fluorescence (Figure S5 in ESI).

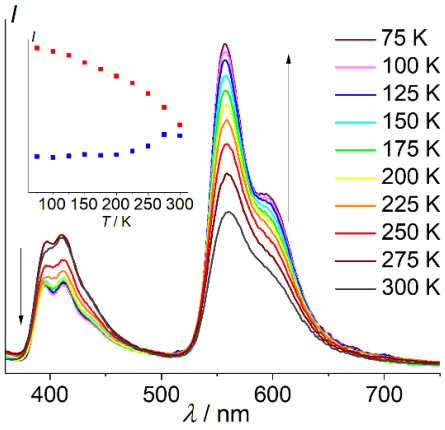

Figure 3. Temperature dependence of emission of a spin-coated film of **8**, 10 ms after switching off the excitation at 340 nm. Inset: Temperature dependence of emission intensity at 566 nm (red) and 412 nm (blue).

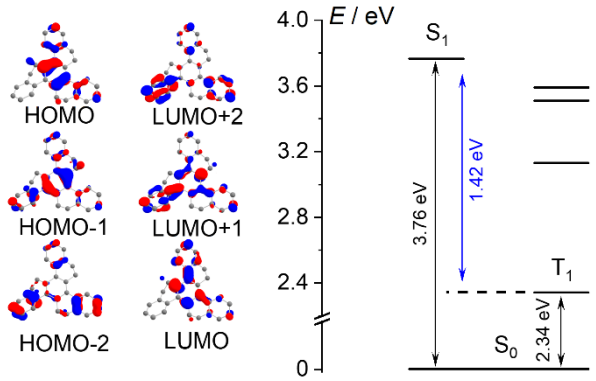

Figure 4. Frontier molecular orbitals of **8** calculated using PBE0/DEF2-TZVP(-F) and energy diagram for the excited states S_1 (3.76 eV), T_1 (2.34 eV), T_2 (3.13 eV), T_3 (3.51 eV) and T_4 (3.59 eV).

We carried out calculations on the electronic structure of **8** using DFT at the PBE0/def2-TVZP(-f) level. The so-obtained geometry for **8**(Figure S6 in ESI) is in good agreement with the structure obtained by single crystal X-ray diffraction, where the average error was 0.44% for bond lengths and 0.65% for bond angles.The calculated HOMO (-2), HOMO (-1), HOMO, LUMO, LUMO (+1) and LUMO (+2) are shown in Figure 4, with an energy diagram for the excited states. The energies ofS_1 and T_1 are relative to the ground state, from theiroptimized geometry, and the energies for the other triplets below S_1were obtained vertically using SOC-TD-DFT. For **8**, the HOMO and HOMO (-1) are degenerate π orbitals located mainly at the central ring, while the LUMO and LUMO (+1) are the respective π^* orbitals. The HOMO (-2) and the LUMO (+2), in contrast, are located at the outer rings, which has implications on the SOC matrix elements (Table 1). The calculated energies of the excited states are in good agreement with the onset of the emission bands, with 3.35 eV (experiment) versus 3.76 eV (theory) for S_1 and 2.33 eV versus 2.34 eV for T_1.

Having the singlet and triplet states of **8**, the SOC matrix elements were calculated using a recently developed approach for SOC TD-DFT (Table 1).[24] For all triplets below S_1, the SOC matrix elements are unusually high for a hydrocarbon. When the average SOC matrix elements between S_1 or S_0 and all triplet states $T_n$with energies between S_1 and $S_0$are examined for **8**, **5**, **7**, benzene and phenanthrene, it is striking that the matrix elements of **8** are about 1½ orders of magnitude greater for $\langle S_1 | \hat{H}_{SO} | T_n \rangle$andabout 2 orders of magnitude greater for $\langle S_0 | \hat{H}_{SO} | T_n \rangle$ than the highest values of the planar arenes (Table S1 in ESI).

Table 1. SOC-TD-DFT data for **8.**

State	$\langle S_0 \lvert H_{SO} \rvert T_n \rangle$[a]	$\langle S_1 \lvert H_{SO} \rvert T_n \rangle$[a]	**Configuration**[b]
T_1	1.19	0.50	H → L (89)
T_2	0.57	0.09	H-1 → L (47) H → L+2 (40)
T_3	1.13	0.16	H-1 → L (40) H → L+2 (41)
T_4	0.51	0.33	H-1 → L+2 (60)

[a] $\sqrt{\Sigma \langle S_i | H_{SO} | T_{j\,(MS=0,\pm1)} \rangle^2}$; [b] Only transitions with contributions larger than 10% are shown (% in parentheses).

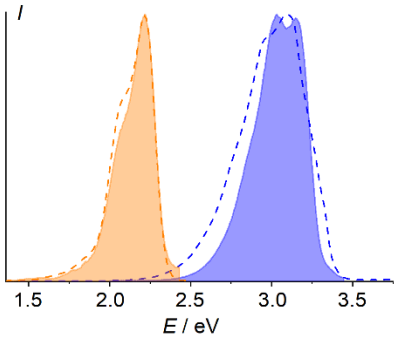

Figure 5. Experimental and predicted (dashed) normalized fluorescence (blue) and phosphorescence (orange) using PBE0/DEF2-TZVP(-F) and the path integral approach. The S_1 0-0 energy difference was blue-shifted by 0.25 eV to match the experimental data.

This can be explained by noting that the triplets have large components of transitions from HOMO-2 and to LUMO+2, which are on the tilted outer rings of **8**. The SOC between these states, with components on the outer rings and the inner ring respectively, are thus increased because there is a change of angular momentum associated with the transition. Due to the twist in**8**, the dihedral angle between these two sets of orbitals makes the coupling through the SOC operator non-zero, as it has the symmetry of a rotation.[30-32] This rotation-dependent SOC is known to occur more commonly in molecules such as benzophenone (**2**) with n-π* excitedstates, which usually involve orthogonal orbitals. In addition, the high triplet energy lowers the non-radiative rate[32] to a point where the phosphorescence rate becomes competitive, allowing for high yields of both persistent RTP and DF.

Combining our path integral approach with the SOC results,[33,34] we could simulate the emission spectra for both the fluorescence and phosphorescence (Figure 5) within a reasonable TD-DFT error. The predicted results are in good agreement with the experimental data, thus corroborating the coexistence of long-wavelength phosphorescence with short-wavelength DF.

In summary, homotruxene**8**, a hydrocarbon with pronounced twist angles between aryl moieties that are sterically stabilized by ethylene bridges, is accessed in a single step from tetralone in gram scale. Itpresents not only persistent room temperature phosphorescence, an extremely rare feature for hydrocarbons, but also delayed fluorescence at room temperature in air, a behavior so far unknown from pure hydrocarbons in crystalline powder or amorphous film.The DF is postulated to result from triplet-triplet annihilation due to its temperature and concentration dependence. DFT modelling of**8**confirmsstrong spin-orbit coupling due to its twisted structure, as well as a high triplet energy that minimizes non-radiativedeexcitationpathways.

Acknowledgements

Weare grateful toCNPq (401028/2016-0), CAPES, FAPESC, INCT-INEO and H2020-MSCA-RISE-2017 (OCTA, #778158) for financial support.

Keywords: Room temperature phosphorescence • Delayed fluorescence • Spin-orbit coupling • Triplet-triplet annihilation • Cyclotrimerization

[1] E. Clar, M. Zander,*Chem. Ber.***1956**, *89*, 749.
[2] M. Zander, Naturwiss. **1960**, *47*, 443.
[3] M. Zander, Naturwiss. **1962**, *49*,7.
[4] M. Zander, Naturwiss. **1965**,*52*,559.
[5] J. L. Kropp, W. R. Dawson, *J. Phys. Chem.***1967**,*71*,4499.
[6] M. Zander, *Z. Naturforsch.***1973**,*28a*,1381.
[7] S. Hirata, *Adv. Optical Mater.***2017**,*5*,1700116.
[8] M. Baroncini, G. Bergamini, P. Ceroni, *Chem. Commun.***2017**,*53*,2081.
[9] W. Z. Yuan, X. Y. Shen, H. Zhao, J. W. Y. Lam, L. Tang, P. Lu, C. Wang, Y. Liu, Z. Wang, Q. Zheng, J. Z. Sun, Y. Ma, B. Z. Tang, *J. Phys. Chem. C***2010**,*114*,6090.
[10] Y. Xiong, Z. Zhao, W. Zhao, H. Ma, Z. He, X. Zhang, Y. Chen, X. He, J. W. Y. Lam, B. Z. Tang, *Angew. Chem. Int. Ed.* **2018**, *57*, 7997.
[11] Y. Kawamura, K. Goushi, J. Brooks, J. J. Brown, H. Sasabe, C. Adachi, *Appl. Phys. Lett.***2005**, *86*, 071104.
[12] A. Fermi, G. Bergamini, R. Peresutti, E. Marchi, M. Roy, P. Ceroni, M. Gingras *DyesPigm.***2014**, *110*, 113.
[13] W. Z. Yuan, X. Y. Shen, H. Zhao, J. W. Y. Lam, L. Tang, P. Lu, C. L. Wang, Y. Liu, Z. M. Wang, Q. Zheng, J. Z. Sun, Y. G. Ma, B. Z. Tang, *J. Phys. Chem. C* **2010**, *114*, 6090.
[14] O. Bolton, K. Lee, H. J. Kim, K. Y. Lin, J. Kim, Nat. Chem. **2011**, 3, 205
[15] L. Yang, X. Wang, G. Zhang, X. Chen, G. Zhang, J. Jiang, *Nanoscale***2016**, *8*, 17422.
[16] M. Baronici, G. Bergamini, P. Ceroni, *Chem. Commun.***2017**, *53*, 2081
[17] E. Lucenti, A. Forni, C. Botta, L. Carlucci, C. Giannini, D. Marinotto, A. Previtali, S. Righetto, E. Cariati, *J. Phys. Chem. Lett.***2017**, *8*, 1894.
[18] M. K. Etherington, J. Gibson, H. F. Higginbotham, T. J. Penfold, A. P. Monkman, *Nature Commun.***2016**,*7*,13680.
[19] C. M. Marian, *WIREsComput. Mol. Sci*. **2012**,*2*,187.
[20] D. B. Clapp, *J. Am. Chem. Soc.***1939**,*61*,523.
[21] K. Claborn, B. Kahr, W. Kaminsky, *Cryst. Eng. Commun.***2002**,*4*,252.
[22] F. R. Ahmed, J. Trotter, *ActaCryst.***1963**,*16*,503.
[23] L. Li, M. Chen, H. Zhang, H. Nie, J. Z. Sun, A. Qin, B. Z. Tang, *Chem. Commun.*, **2015**, *51*, 4830.
[24] B. Stevens, E. Hutton, Proc. Phys. Soc. **1963**,*81*,893.
[25] C. Huang, W. Fu, C.-Z. Li, Z. Zhang, W. Qiu, M. Shi, P. Heremans, A. K.-Y. Jen, H. Chen, J. Am. Chem. Soc. **2016**,*138*,2528.
[26] S. Zhao, L. Kang, H. Ge, F. Yang, C. Wang, C. Li, Q. Wang, M. Zhao, *Synth.Commun.***2012**, *42*, 3569.
[27] A. Pyrko, *Zh. Org. Khim.***1992**,*28*,215.
[28] S. Hagen, L. T. Scott, *J. Org. Chem.***1996**,*61*,7198.
[29] Z. He, W. Zhao, J. W. Y. Lam, Q. Peng, H. Ma, G. Liang, Z. Shuai, B. Z. Tang, *Nature Commun.***2017**,*8*,416.
[30] M. A. El-Sayed, *J. Chem. Phys.***1963**, *38*, 2834.

[31] S. K. Lower, M. A. El-Sayed, *Chem. Rev.***1966**, *66*, 199.
[32] N. J. Turro, V. Ramamurthy, J. C. Scaiano, *Modern Molecular Photochemistry of Organic Molecules*, University Science Books, Sausalito **2010**.
[33] B. de Souza, F. Neese, R. Izsák, *J. Phys. Chem.* **2018**, *148*, 034104.
[34] B. de Souza, G. Farias, F. Neese, R. Izsák, *J. Chem. Theo. Comp.***2019**, *15*, 1896.

Supplementary Information

Photophysical and theoretical methods

Photoluminescence spectra from chloroform solution, from thin solid film and from the crystalline powder were obtained using a Varian Cary Eclipse Fluorescence spectrophotometer. For temperature variation measurements a closed vacuum cryostat (VC) (by Janis Research) was used, with helium compressor (model HC-4E, SHI Cryogenics Group), and temperature controller (model 336, Lake Shore Cryotronics). Absolute quantum yields in the solid were measured with a Hamamatsu Photonics Absolute Quantum Yield Measurement System model c9920-02G, using the integrating sphere method. Photoluminescence decay times at temperatures from 10 to 300K were measured using a Hamamatsu TM series CCD mini spectrometer coupled to an optical fiber probe with a dedicated waveguide for irradiation that was immersed in a liquid helium bath cryostat. Thin solid spin coated films were obtained from chloroform solution (5 mg/mL) at 1500 rpm during 30s. AFM measurements were done with a NanosurfFlexAFM operating in tapping mode under ambient conditions with a scanning rate of 1.0 Hz and 512 pixels × 512 pixels. The pola-rizing optical microscopy image of a spin-coated film scratched with a needle was captured with a DP73 Camera coupled to a Olympus BX53 microscope.

Geometry optimization of **8** was carried out in vacuum, using the Orca 4.1[1] software package and DFT with the PBE0 functional[2,3] and the DEF2-TZVP(-F) basis set for all atoms.[4-6] Dispersion effects were included using Grimme's D3 correction with Becke-Johnson (BJ) damping.[7,8] The RIJCOSX algorithm was employed to accelerate the evaluation of the functionals, using the resolution of identity approximation for the Coulomb part (RIJ), and the chain of spheres approach for the Fock exchange (COSX).[9,10] RIJCOSX requires the specification of an auxiliary basis set for the Coulomb part and that of a numerical integration grid for the exchange part discussed elsewhere. The vibrational frequencies computed on the optimized geometry of **8** included no imaginary ones. Time-dependent density functional theory (TD-DFT) under Tamn-Dancoff approximation[11] (TDA) was employed to obtain the first 10 singlet excited states, using the same calculation protocol to optimize the geometry and calculate the Hessian of the first excited state. The first triplet was optimized from the ground state of UKS calculation. Images of the complex geometries were obtained using the Chemcraft program.[12] SOC on top of the TD-DFT results was included by using quasi-degenerate perturbation theory. The SOC integrals used here are the ones calculated using a mean-field named RI-SOMF(1X) described elsewhere.[13] In order to compute the fluorescence and phosphorescence spectra, the path integral approach implanted in the ORCA_ESD module[14,15] was used with the same protocol as above for the SCF and TD-DFT, except for the larger grids GRID4 and GRIDX4. Defaults were used otherwise unless mentioned. The normal modes chosen for the model were those with frequencies above 300 cm^{-1} and a Gaussian line shape was set, with a line width of 400 cm^{-1} for phosphorescence and 150 cm^{-1} for fluorescence.

[1] F. Neese, *Wiley Interdiscip. Rev. Comput. Mol. Sci.***2017**, 8, e1327.
[2] J. P. Perdew, K. Burke, M. Ernzerhof, *Phys. Rev. Lett.***1996**, 77, 3865.
[3] J. P. Perdew, K. Burke, M. Ernzerhof, *Phys. Rev. Lett.***1997**, 78, 1396.
[4] A. Schäfer, H. Horn, R. Ahlrichs, *J. Phys. Chem.* **1992**, 97, 2571.
[5] A. Schäfer, C. Huber, R. Ahlrichs, R. *J. Phys. Chem.* **1994**, 100, 5829.
[6] F. Weigend, R. Ahlrichs, *Phys. Chem. Chem. Phys*. **2005**, 7, 3297.
[7] S. Grimme, J. Antony, S. Ehrlich, H. Krieg, *J. Chem. Phys.***2010**, 132, 154104.
[8] S. Grimme, S. Ehrlich, L. Goerigk, *J. Comput. Chem.***2011**, 32, 1456.
[9] R. Izsák, F. Neese, *J. Phys. Chem.* **2011**, 135 , 144105.
[10] R. Izsák, F. Neese, W. Klopper, W. *J. Phys. Chem.* **2013**, 139, 094111.
[11] T. Petrenko, S. Kossmann, F. Neese, *J. Chem. Phys*. 2011, 134, 054116.
[12] www.chemcraftprog.com.
[13] F. Neese, *J. Chem. Phys*. **2005**, 122, 034107.
[14] B. de Souza, F. Neese, R. Izsák, *J. Chem. Phys.* **2018**, 148, 034104.
[15] B. de Souza, G. Farias, F. Neese, R. Izsák, *J. Chem. Theo. Comp.* **2019**, *15*, 1896.

Lifetimemeasurements

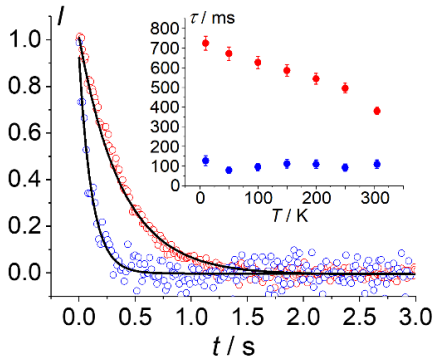

Figure S1. Lifetime of delayed fluorescence (in blue) and phosphorescence (in red) of crystalline **8** at room temperature. The solid lines indicate mono-exponential fitting. The inset shows the lifetime values as a function of temperature.

Concentrationdependenceofphotoluminescence in solution

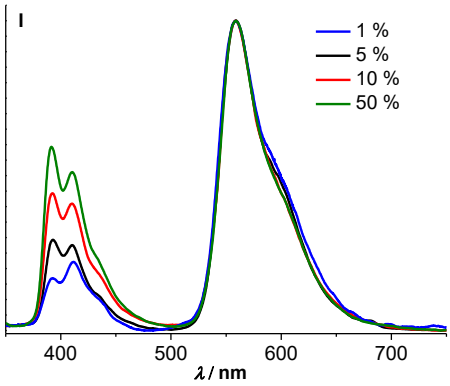

Figure S2. Normalized emission at different concentrations in PMMA matrix at room temperature, 10 ms after switch-off. Excitation at 340 nm in spin-coated film. The relative increase of DF with respect to RTP on increasing concentration is coherent with a TTA (i.e. bimolecular) mechanism.

Synthesis of homotruxene 8

A solution of titanium tetrachloride (3 mL, 189.7 g/mol, 1.726 g/mL, 27 mmol) in DCM (25 mL) was added dropwise with stirring under exclusion of moisture to a solution of 1-tetralone (15 g, 146.2 g/mol, 103 mmol) in DCM (25 mL). The solvent was evaporated through a Dean-Stark receiver whilst the temperature was increased to 150°C, and the partially solidifying residue was stirred vigorously at 150°C for 16 h. After cooling the residue to room temperature, it was dissolved by stirring in a biphasic mixture of DCM and 5% aqueous hydrochloric acid. The organic phase was separated and dried over sodium sulphate. The solvent was evaporated and the residue was dissolved in a small amount of hot chloroform and separated by column chromatography in a 1:1 mixture of petroleum ether and DCM. The first-eluted product was dissolved in the minimum amount of chloroform and crystallized by adding acetone, yielding 1.16 g of **8**. Adding ethanol yielded a further, slightly less pure crop of 0.25 g after 3 d in the freezer. Combined yield: 1.41 g (384.5 g/mol, 3.67 mmol, 10.7 %).

When the reaction was conducted with 4 mL instead of 3 mL of $TiCl_4$, only 0.96 g (7.3 %) of **8** were obtained under otherwise similar conditions, and using either 2 mL or 6 mL of $TiCl_4$ gave only traces of **8**. Increasing the reaction temperature to 200°C led to 1.31 g (≤9.9 %) of impure **8** that we could not purify satisfyingly.
^{1}H NMR ($CDCl_3$, 400MHz, 22°C): δ = 7.47 (dd, 2Hz, 8Hz, 3H), 7.32 (dd, 2Hz, 8Hz, 3H), 7.28 (dt, 2Hz, 8Hz, 3H), 7.26 (dt, 2Hz, 8Hz, 3H), 3.35 (broad, 3H), 2.94 (broad, 3H), 2.73 (broad, 3H), 2.63 (broad, 3H) ppm. ^{13}C NMR ($CDCl_3$, 100MHz, 57°C): δ = 140.2, 136.1, 135.2, 133.4, 129.1, 126.8, 126.7, 125.6, 30.7, 30.6 ppm. FD HRMS: *m/z*calcd for $C_{30}H_{24}$ $[M]^+$: 384.1873; found: 384.1880. EA: calcd for for $C_{30}H_{24}$: 93.71 %C, 6.29 %H; found: 93.61 %C, 6.35 %H. Mp.:>270°C.

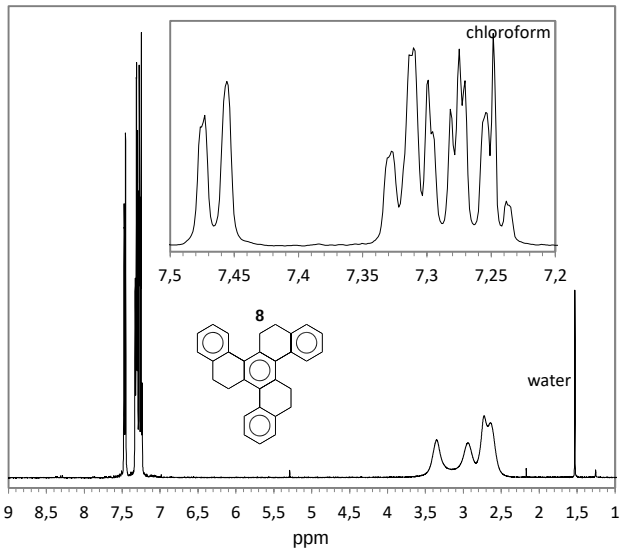

Figure S3a. ^{1}H-NMR spectrum of **8** at 22°C (400 MHz, $CDCl_3$).

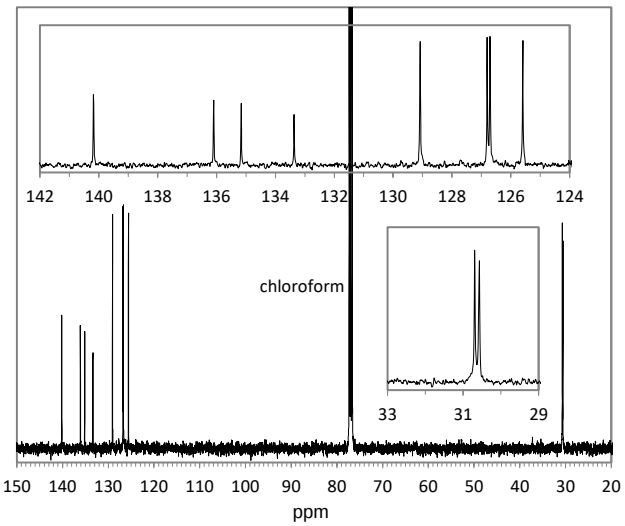

Figure S3b. ^{13}C-NMR spectrum of **8** at 57°C (100 MHz, $CDCl_3$).

Temperature dependence of ^{1}H-NMR spectra

In solution at room temperature (around 20°C), the ^{1}H-NMR spectrum of homotruxene**8** exhibits four strongly broadened aliphatic signals. This indicates that the four aliphatic bridge protons are distinct, as the bridge adopts a dissymmetric conformation with respect to the central benzene plane. As the peaks corresponding to one of the methylene groups are at 400 MHz separated by about 0.4 ppm, i. e. $\Delta\nu$ = 160 Hz, and those of the other methylene group by about 0.2 ppm, i. e. $\Delta\nu$ = 80 Hz, and as the former merge to a single broad peak at about 40°C, and the latter at about 30°C, the exchange rate $1/\tau$ at room temperature between the two opposite bridge conformations can be estimated: From $\tau_{coalescence} = (\sqrt{2} \times \pi \times \Delta\nu)^{-1}$[16] and from the observed difference of coalescence temperatures of *c.* 10K that correspond to a factor of about two between the two $\Delta\nu$ values, the exchange rate must be of the order of 200 Hz at room temperature. At subambient temperatures, the four broad peaks resolve into two doublets and two triplets, each with *J* = 14 Hz, i. e. both geminal couplings and one of the four vicinal couplings have this same large coupling constant, whereas the three remaining vicinal couplings are small. Above *c.* 80°C, the two methylene signals obtained by the mergers at 30 and 40°C resolve into triplets with a usual vicinal aliphatic coupling of *J* = 7 Hz. The reported room temperature ^{1}H-NMR spectrum of 5,6-dihydrochrysene,[17] arguably the simplest known analog with a similar ethylene bridge between two non-identical linked arene units, shows two 7 Hz triplets, without indication of the conformational persistence observed with **8**. We therefore assume that the steric congestion in **8** between the inner methylene and the outer benzene ring of the next branch is causing this stabilization.

[16] R. G. Bryant, *J. Chem. Educ.* **1983**, *60*, 933.
[17] F. Nador, Y. Moglie, C. Vitale, M. Yus, F. Alonso, G. Radovoy, *Tetrahedron***2010**, *66*, 4318.

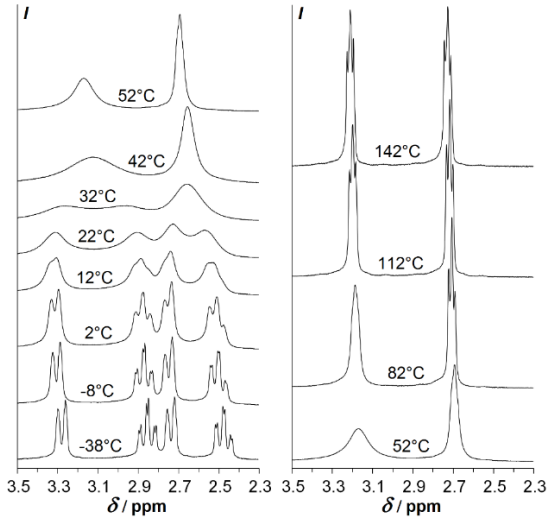

Figure S3c. Temperature dependence of the aliphatic part of the ^{1}H-NMR spectrum of **8** (-38 to 42°C in d_2-DCM, 52 to 142°C in d_2-tetrachloroethane, 400MHz). At low temperature, two broadened doublets of *J* = 14 Hz and two doubled triplets of J_t= 14 Hz and J_d = 4 Hz are observed, which transform over a range of *c.* 100 K into two triplets of *J* = 7 Hz at high temperature.

Morphology of spin-coated film

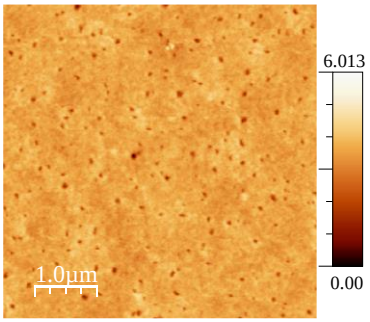

Figure S4. Top: AFM image (5 µm× 5 µm) of a film spin-coated onto glass from chloroform solution, exhibiting a RMS roughness of 0.35 nm. Color scale in nm. Bottom: Brightness- and contrast-enhanced polarizing optical microscopy image with slightly uncrossed polarizers of a film spin-coated onto glass from chloroform solution, showing scratches in the organic layer made by a needle, to illustrate the smooth and non-birefringent nature of the film. The bar represents 10 µm.

Photophysical mechanism

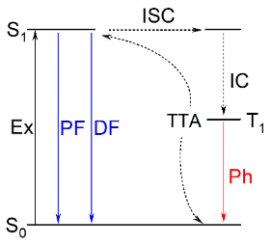

Figure S5. Proposed photophysical mechanism. Ex = excitation, PF = prompt fluorescence, DF = delayed fluorescence, ISC = intersystem crossing, IC = internal conversion, Ph = phosphorescence, TTA = triplet-triplet annihilation.

Single crystal X-ray diffraction

The crystallographic data were collected with a Bruker APEX II Quasar diffractometer, equipped with an Oxford Cryostream 700plus cryostat and an Incoatec microfocus sealed-tube of monochromatized MoKα radiation. A single crystal of homotruxene **8** obtained from acetone solution was coated with Paratone N-oil and mounted on a fiber loop, followed by data collection at 120 K. The program SAINT was used to integrate the data, which was thereafter corrected using SADABS.[18] The structure was solved using SHELXS-2013 and refined by a full-matrix least-squares method on F^2 using SHELXL-2014. [19]All non-hydrogens were refined anisotropically. Hydrogen atoms were assigned to ideal positions and refined isotropically using suitable riding models. A lattice acetone molecule was found to be disordered on three equivalent positions. Hydrogen atoms of this disordered acetone were not introduced, but are taken into account in the compound formula. The CIF file has been deposited at the Cambridge Crystallographic Data Centre as supplementary publication no. CCDC 1894137.
$C_{33}H_{30}O$, trigonal, *P-3* (no. 147), $a = b = 13.5618(11)$, $c = 7.4947(8)$, $V = 1193.8(2)$ Å^3, $Z = 2$, $T = 120$ K, 46070 reflections measured, 1606 unique ($R_{int} = 0.0540$), GoF = 1.105, $R_1 = 0.0556$, wR_2 (all reflections) = 0.1910.

[18] G. M. Sheldrick, SADABS Version 2.03, Bruker Analytical X-Ray Systems, Madison, WI, 2000.
[19] G. M. Sheldrick, *ActaCryst. C71*, **2015**, 3.

Theoretical modelling

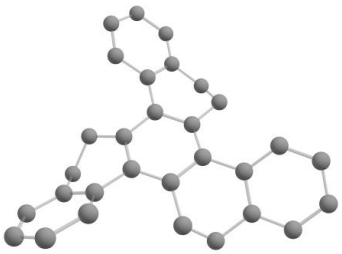

Figure S6. Optimized structure to the ground state at PBE0/DEF2-TZVP(-F) level.

Table S1. SOC-TD-DFT data for **8**, **5**, **7**,benzeneand phenanthene

Matrix element	8	5	7	benzene	phenanthrene
$\langle S_0\|H_{SO}\|T_n\rangle^a$	0.85	0.00	0.01	0.00	0.00
$\langle S_1\|H_{SO}\|T_n\rangle^a$	0.27	0.00	0.00	0.00	0.01

[a] $\sqrt{\sum \langle S_i|H_{SO}|T_{j\,(MS=0,\pm1)}\rangle^2}$.

Table S2. Cartesian coordinates for the optimized structure of the ground state of **8** using PBE0/DEF2-TZVP(-F).

C	-3.35596048190255	0.15170212525828	0.16538314827985
C	-2.24902361163766	1.00266522179008	-0.04162776681845
C	-0.96607174102816	0.50479856034111	0.01667012462777
C	-3.15558821140355	-1.32375295155290	0.12151466972311
C	-1.84453386755050	-1.82967996703485	0.22250805590343
C	-0.74115050310473	-0.97573018361361	0.12911167791317
C	-4.60223574652459	0.72865192338621	0.77197482217554
C	-4.30796412010087	2.04534512830729	1.50182350759277
H	-5.04506174387719	-0.00016273715485	1.45437027165453
H	-5.37076226933014	0.92400061676948	0.01224711262548
C	-3.60520022984199	2.98261651675830	0.56330580354959
H	-3.66531136576840	1.83460455299883	2.36398840199353
H	-5.22784115499872	2.49207729114415	1.88221882312536
C	-2.55330332756482	2.44745382866843	-0.19464547105964
C	0.24224159062481	1.38603509237019	0.10341412593216
C	0.64712400042603	-1.41861008662467	0.07832949663549
C	1.26865893828522	0.79181808217569	1.07217587652470
H	-0.04690282577100	2.38693518277452	0.42065747594828
H	0.72614649115547	1.49547499871872	-0.87602177085063
C	1.66073314220669	-0.57142360954751	0.59427341219438
H	0.82369828000100	0.73981750109475	2.07174441544340
H	2.14582286168782	1.43686956988455	1.14235906835612
C	-4.26252541427772	-2.21078232934416	-0.09766296586154
C	-4.16315483306570	-3.56732542021994	0.32158870025301
C	-2.91429398784084	-3.95369925335363	1.04809873734647
C	-1.70390234460638	-3.33224064071647	0.36269088298889
H	-0.79497000523844	-3.57462385986720	0.90989355100923
H	-1.60809495230997	-3.78933257341192	-0.62836978768723
H	-2.81165161702644	-5.03933311016940	1.09048029177866
H	-2.97233623776914	-3.58821542207907	2.08111720714230
C	-3.96983193563734	4.31319378239295	0.39736819400445
C	-3.29979664183584	5.12398145013462	-0.51280637172894
C	-2.26154946195821	4.59545984862995	-1.27055278101950
C	-1.89747105579492	3.26390876933983	-1.11641423758695
H	-1.11531099071406	2.84802686426637	-1.73602046903657
H	-4.78702423471347	4.71660251270541	0.98384536658295
H	-1.74412713637781	5.21405783577942	-1.99264404600161
H	-3.60139981445364	6.15529708589977	-0.64555283043467
C	-5.45690927341383	-1.81433233745557	-0.74689092770075
C	-6.47713892035275	-2.71691444459170	-0.97785963727185
C	-6.36238748288808	-4.04115518157866	-0.55989767156502
C	-5.19595567876939	-4.45188581714837	0.08956264262662
H	-5.55933749348944	-0.80300252677272	-1.10822136207153
H	-7.36923780408767	-2.38722089858474	-1.49556198326120
H	-7.16421880186808	-4.74502603751219	-0.73990741421813
H	-5.09837863035513	-5.47663411467060	0.42860756031315
C	1.06300403339819	-2.63338276752288	-0.50503772731523
C	2.98487599675704	-0.98400943949170	0.60257154580416
C	3.35994679261585	-2.21586752652013	0.07855674022663
C	2.38817551729471	-3.02660694752902	-0.49993933376057
H	0.34533498419663	-3.25457009103498	-1.01218595173731
H	3.73543696100705	-0.32377207782869	1.02139113968628
H	2.66892921133231	-3.96342744946450	-0.96419446443314
H	4.39637714826038	-2.52752453919221	0.09470212145899

Table S3. Cartesian coordinates for the optimized structure of the S_1 state of **8** using PBE0/DEF2-TZVP(-F).

C	-3.37272672941669	0.13349737978566	0.08919931660136
C	-2.25819628153727	1.02018170954494	0.02058379595051
C	-0.94227835794533	0.49585108493719	0.09352463375726
C	-3.17050638230144	-1.26989548293073	0.05645543310079
C	-1.84564045055451	-1.79064293935932	0.13929531569238
C	-0.73299275272726	-0.91397133216161	0.06340190438070
C	-4.72413679269892	0.73559581869262	0.30422337352620
C	-4.61776045569226	2.00061558841811	1.14614551386867
H	-5.38552691205882	0.01003641807035	0.77808992240609
H	-5.18967949917536	1.00881903808872	-0.65482333014832
C	-3.71089530449811	2.96302731459334	0.45860749296708
H	-4.21396595253919	1.73665934412382	2.13121810453528
H	-5.60277317218902	2.44522365639269	1.30363006549937
C	-2.53045692165642	2.43705149188169	-0.11720409077563
C	0.25069508697109	1.36915791011096	0.31740872973341
C	0.63128513358563	-1.39049821694409	-0.04377622931607
C	1.28413050929094	0.66055915611247	1.18367727647808
H	-0.05737426353268	2.30953934403610	0.77501167740910
H	0.73377947153543	1.62777420050041	-0.63696432363855
C	1.67147077185634	-0.61984606670667	0.52676114972895
H	0.84523230706933	0.46160516243614	2.16893982675326
H	2.16044840118246	1.29381701521724	1.33739934226502
C	-4.26151046737898	-2.21710762841117	-0.05848892289014
C	-4.12685548851305	-3.48907947961903	0.54631963108104
C	-2.84905004210608	-3.76613980451598	1.26162141415778
C	-1.68876430684839	-3.25107705208235	0.41982091079351
H	-0.73661857863589	-3.43415036322212	0.91934992484849
H	-1.66914920935361	-3.83279541306035	-0.51343503421974
H	-2.74121317431494	-4.83457926801467	1.45898057615704
H	-2.84072568483982	-3.25022281854076	2.22925094396769
C	-3.99414957276598	4.31109779584888	0.35673798243212
C	-3.14630643095322	5.17158798792080	-0.33203861156076
C	-2.00541907138218	4.66003315753639	-0.94199520385070
C	-1.70166758306932	3.31820294912262	-0.83846337380428
H	-0.83377112910952	2.93198337482033	-1.35507227653769
H	-4.90004597642636	4.69466250431737	0.81457467441482
H	-1.35695289648231	5.31384552518003	-1.51370740586212
H	-3.38553370769505	6.22519326829635	-0.41157682162087
C	-5.43387319532109	-1.96032056951275	-0.79585482175527
C	-6.43591088989237	-2.90291205547350	-0.89355843690645
C	-6.30753652113530	-4.13518275964040	-0.26018441751011
C	-5.14385810620742	-4.41850592983195	0.44707531882171
H	-5.53382267410144	-1.02674977867663	-1.33215975901924
H	-7.32220046955636	-2.68295706412658	-1.47740015779282
H	-7.09565344945592	-4.87492937114521	-0.33356983647911
H	-5.02236767637050	-5.38510217645775	0.92479944597963
C	0.98518608176791	-2.56485583219688	-0.73477759496379
C	2.98116023532691	-1.05159649416468	0.44751336847793
C	3.30734680355793	-2.23323641844632	-0.20935895944100
C	2.29893450604520	-2.97667952937758	-0.81474093530533
H	0.22137804262380	-3.13119454593160	-1.24864236316359
H	3.76219409563279	-0.45138847276169	0.90258176223454
H	2.54419958306893	-3.87986065329265	-1.36127612485873
H	4.33901550092374	-2.55899067938014	-0.26659979659959

Table S4. Cartesian coordinates for the optimized structure of the T_1 state of **8** using PBE0/DEF2-TZVP(-F).

C	-3.32996862523332	0.13681920835382	0.24310649284868
C	-2.22833849193520	0.99809636162693	-0.03012040031688
C	-0.96251526256650	0.49362510426675	-0.02451466994678
C	-3.13540291771873	-1.32772957519700	0.11608889801751

C	-1.84232331968032	-1.84468825475530	0.18199325036386
C	-0.73256921993984	-0.97597809804235	0.12042818388344
C	-4.49919473054222	0.68763173094472	0.98989463927586
C	-4.17250656884387	2.03822519991510	1.62508670805571
H	-4.81260422270410	-0.03464526358749	1.75174951394748
H	-5.37539641212301	0.80853088875187	0.33646062029035
C	-3.57486627875719	2.95319196746960	0.60213602560876
H	-3.44690359572868	1.87795607438296	2.43189668030614
H	-5.06348014250768	2.48138952249551	2.07456295175514
C	-2.56328824646855	2.42111255772035	-0.20713746935831
C	0.24762154591240	1.36668939635018	-0.05028143376975
C	0.65017319719177	-1.41049412725955	0.12281213266342
C	1.25596763662642	0.86646912927145	0.97700349682338
H	-0.03530434078340	2.39913830163445	0.15308954506260
H	0.72959219857939	1.34689892394308	-1.03713992090616
C	1.64454584802592	-0.53051359641362	0.62265648060968
H	0.80057486677665	0.91311319066669	1.97303874312793
H	2.14195190436610	1.50475419572077	0.99531076192705
C	-4.26023448683954	-2.18781747508462	-0.12788430991129
C	-4.17611051635596	-3.55629733187357	0.21529558733898
C	-2.91843337163131	-4.01036486771584	0.87292620085296
C	-1.70858140517493	-3.34362829884795	0.24432541403819
H	-0.81245963245950	-3.61338770083376	0.80320480973277
H	-1.57865653986779	-3.74337093157377	-0.76947000410124
H	-2.82721895689342	-5.09682575124641	0.79855307907231
H	-2.95651573205827	-3.75509714452364	1.94053619556553
C	-3.97832691865553	4.26722900332450	0.41749890466558
C	-3.39211014296335	5.05552793670795	-0.56335623988483
C	-2.39657433751294	4.52697896196801	-1.37182101070217
C	-1.99164889225108	3.21300700614981	-1.19869801524697
H	-1.24462010494493	2.78518918436140	-1.85586746317805
H	-4.76070385875439	4.67738936898400	1.04771093457779
H	-1.94421420445483	5.13274688175311	-2.14803087739562
H	-3.72540522029793	6.07630737476358	-0.71013602231729
C	-5.44861026954595	-1.72847603414879	-0.72939900932336
C	-6.49752092851704	-2.59154184237717	-0.97538966821731
C	-6.40788733714011	-3.92991642428260	-0.61500700402404
C	-5.23962420073421	-4.40127072727771	-0.02262295573613
H	-5.52375512146301	-0.69684515750948	-1.04465952693369
H	-7.39338363556733	-2.21758442432037	-1.45769816498291
H	-7.23623533166976	-4.60337448956107	-0.79928088874095
H	-5.16086236562601	-5.44399764750035	0.26761055511802
C	1.09140884702311	-2.65428134360297	-0.37204067970435
C	2.96092942061339	-0.94590384717617	0.71715340858959
C	3.35490136448901	-2.20661630307817	0.29245017087078
C	2.41135682287850	-3.04623635364005	-0.28434163016451
H	0.39943978491140	-3.30536489434466	-0.88136966288903
H	3.69608143795635	-0.25900071335054	1.12374752815074
H	2.70969025713668	-4.00689625289735	-0.68775374346578
H	4.38871075442469	-2.51872259950419	0.38222285807728